

Fully developed periodic turbulent pipe flow. Part 2. The detailed structure of the flow

By **B. R. RAMAPRIAN**

Iowa Institute of Hydraulic Research, The University of Iowa

AND **S. W. TU**

Bechtel Civil and Mineral Inc., San Francisco, California

(Received 18 February 1982 and in revised form 19 July 1983)

The main experimental results of the study of periodic turbulent pipe flow have been described in Part 1 of this report. In this second part, these experimental data are examined in greater detail to understand the effect of imposed oscillation on the flow structure, at moderate to large oscillation frequencies. Data on phase and amplitude and energy spectrum are used to study the effect of the imposed oscillation on the turbulence structure at these interactive frequencies of oscillation. Additional experiments which were performed to study the effect of oscillation frequency on the flow structure are also reported. Based on the present observations as well as on the data from other sources, it is inferred that turbulent shear flows respond very differently from laminar shear flows to imposed unsteadiness. A turbulent Stokes number relevant for characterizing the unsteady turbulent shear flows is identified and used to classify such flows.

1. Introduction

In Part 1 (Tu & Ramaprian 1983) of this two-part report the main results obtained from an experimental study of oscillatory flow of water in a long circular pipe (of diameter D) at a mean Reynolds number Re of about 50000 have been presented. These results were obtained at two oscillation frequencies f_{os} of 0.5 and 3.6 Hz with oscillation amplitudes 64 and 15 % respectively. The sinusoidal oscillation of the flow around the mean was produced in each case by regulating the exit area at the downstream end by a suitably designed rotating sleeve valve. Details of the experimental apparatus as well as the instrumentation for the measurement and processing of the velocity and wall-shear-stress data are given in Part 1. In the same paper are also given results obtained from numerical calculations using a quasi-steady turbulence model.

In this paper the basic experimental data described in Part 1 are further processed to obtain more detailed information on the structure of periodic pipe flow. The aspects studied include phase and amplitude characteristics, and energy spectrum of the longitudinal turbulent intensity. Also, the results of a third series of experiments (in addition to those described in Part 1), in which the oscillation frequency was varied from 0.5 to 3.0 Hz, are discussed. In these experiments, the amplitude of modulation was maintained approximately constant so that the effect of oscillation frequency could be studied in isolation.

2. Experimental and data-reduction procedures

2.1. Amplitude and phase calculations

The *imposed* cross-sectional-average velocity $\langle U_m \rangle$ in the present experiments is given by

$$\langle U_m \rangle = \bar{U}_m [1 + \gamma_{U_m} \cos(2\pi f_{os} t)], \quad (1)$$

where \bar{U}_m is the time-mean cross-sectional-average velocity, γ_{U_m} is the relative amplitude of cross-sectional-average velocity and f_{os} is the frequency of oscillation. If we consider only the fundamental (dominant) frequency, the ensemble-averaged velocity $\langle U \rangle$ at any point at radius r (or distance y from the wall) and at time t can then be written as

$$\langle U \rangle(y, t) = \bar{U}(y) [1 + \gamma_U \cos(\omega t + \phi_U)], \quad (2)$$

where \bar{U} is the time-mean velocity at the point, γ_U is the relative amplitude of the ensemble-average velocity and $\phi_U(y)$ is the phase lead with respect to $\langle U_m \rangle$. Higher-harmonic components in the velocity were found to be very small. This was possible because of the careful design of the sleeve profile. However, it has been shown in Part 1 that other ensemble-average properties such as wall shear stress $\langle \tau_w \rangle$, longitudinal turbulent intensity u'_p ($= \langle u^2 \rangle^{\frac{1}{2}}$) and Reynolds shear stress $-\langle uv \rangle$ (where v is turbulent velocity in the radial direction) showed some distortions from a sinusoidal variation. Nevertheless it was decided to study only the properties of the fundamental frequency even in these cases. Hence we now introduce the general expression

$$\langle X \rangle \approx \bar{X} [1 + \gamma_X \cos(\omega t + \phi_X)], \quad (3)$$

where γ_X and ϕ_X are the amplitude and phase angle of the property X , and X stands for U , τ_w or $-uv$, and $\omega t = 2\pi f_{os} t = \theta$ represents the phase position in the cycle relative to the variation of $\langle U_m \rangle$. For the longitudinal turbulence intensity, we define

$$u'_p = \bar{u}'_p [1 + \gamma_{u'_p} \cos(\omega t + \phi_{u'_p})], \quad (4)$$

where

$$\bar{u}'_p = \frac{1}{2\pi} \int_0^{2\pi} u'_p d\theta. \quad (5)$$

2.2. Series 3 experiments

Series 2 experiments described in Part 1 were performed at two oscillation frequencies with the modulation of $\langle U_m \rangle$ being 15% for 3.6 Hz and 64% for 0.5 Hz respectively. In the third series of experiments (also performed at $Re = 50000$) the modulation of the discharge was kept approximately the same (about 25%) while the oscillation frequency was varied over a wide range. These experiments were conducted primarily to obtain information on the influence of oscillation frequency on the behaviour of the flow at the wall and near the centreline. Two different sleeve profiles were used in these experiments. These were designed to produce an exact sinusoidal modulation of discharge at $f_{os} = 1.0$ Hz and 2.5 Hz. The same sleeve profiles were also used for experiments at neighbouring frequencies of the designed frequency by assuming that the change in the amplitude of modulation and distortion are not large at these off-design frequencies. In all these cases, measurements were made (using laser-Doppler anemometry) at the centreline for velocity and at the wall (using a flush-mounted hot-film gauge) for the wall shear stress. Distribution of velocity across the pipe was not measured in these experiments. The same data acquisition procedures were used as those described in Part 1 for the other series of experiments.

2.3. Measurement of energy spectra

Spectral density functions of the time-averaged Reynolds normal stress u'^2 , where

$$u'^2 = \frac{1}{2\pi} \int_0^{2\pi} \langle u^2 \rangle d\theta, \quad (6)$$

were obtained at several locations across the pipe in the periodic flow and compared with those obtained in steady flow at the mean Reynolds number. In each case, two spectra were obtained at each location – one spectrum with a fine resolution giving the energy distribution in the lower frequency range, and the other a broad spectrum extending to higher frequencies. Later these two spectra were patched together to construct one composite spectrum that provided the required resolution and bandwidth. Also spectra were obtained both before and after the periodic component was removed from the LDA output.

The spectra were obtained by the fast Fourier transform (FFT) technique using 1024 points in the time-series data output by the LDA. The spectra were averaged over 95–190 realizations. Standard procedures (see e.g. Bendat & Piersol 1971) for sampling, low-pass filtering and smoothing were used. Further, the spectral measurements obtained in steady pipe flow at a Reynolds number of 50000 were compared with the data of Lawn (1971) and were found to be in good agreement. The experimental procedures as well as several tests to ensure the accuracy of the spectral measurements are described in Ramaprian & Tu (1982).

3. Results and discussion

3.1. Amplitude and phase results for the ensemble-averaged properties

3.1.1. Velocities

Figure 1(a) shows the amplitude distributions of velocity across the pipe for the two frequencies of oscillation. The quantity plotted is the amplitude of local velocity $\gamma_U \bar{U}$ normalized by the amplitude of cross-sectional-averaged velocity $\gamma_{U_m} \bar{U}_m$. It is seen that an overshoot in amplitude occurs in both the experiments. The location η_s of the overshoot from the wall differs because of the difference in the oscillation frequencies imposed. At lower frequency, η_s is larger. It is also seen that, at the higher frequency, the normalized amplitude is nearly unity beyond $\eta \approx 0.4$, indicating that the flow in this region oscillates almost like a solid body. In the same figure, the corresponding amplitude distribution calculated for both laminar flow (using the exact solution from Uchida 1956) and turbulent flow using the quasi-steady numerical method mentioned in Part 1 are shown. First, on comparing the experimental results with theoretical results for laminar periodic flow at the same frequency, significant differences can be observed. At both oscillation frequencies, the laminar flow exhibits sharper peaks than the turbulent flow. Also, the peaks (or overshoots) occur closer to the wall in the case of the laminar flow. In fact, at 0.5 Hz the contrast between laminar and turbulent flows is quite striking, with the turbulent flow exhibiting a very diffused peak and the maximum amplitude occurring around $\eta = 0.5$. Somewhat similar observations were made by Ramaprian & Tu (1980) at low Reynolds number. However, the contrast between turbulent and laminar flow was not as clear in the earlier experiments as in the present experiments, and hence the results were not conclusive. This is due to the very low (transitional) Reynolds number of the flow in the earlier experiments. Likewise, other experiments such as those of Hino, Sawamoto & Takasu (1976) and Binder & Kueny (1981), which were

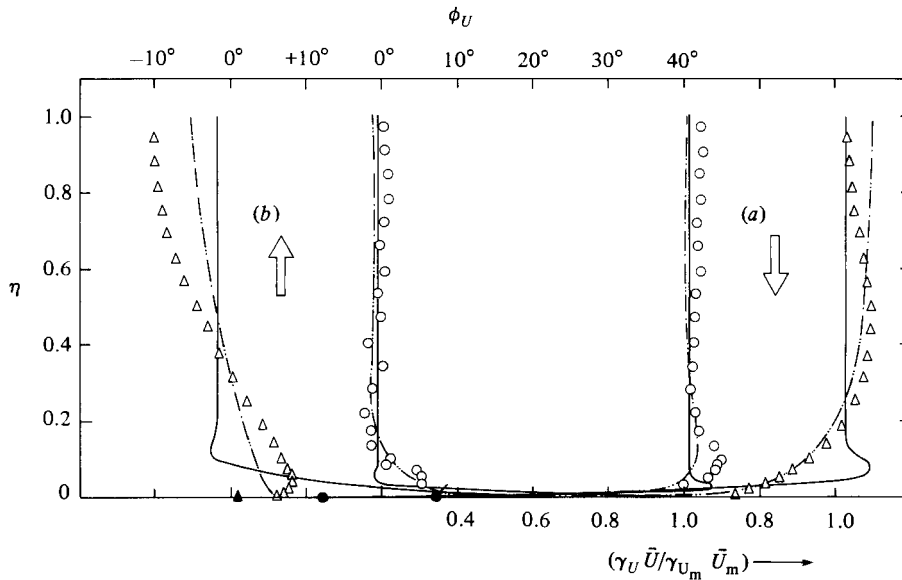


FIGURE 1. Amplitude and phase of the ensemble-averaged velocity: (a) amplitude; (b) phase; \circ , 3.6 Hz; \triangle , 0.5 Hz; filled symbols represent wall-shear-stress data: \bullet , 3.6 Hz (for fundamental frequency); \blacklozenge , 3.6 Hz (from shear-stress maximum); \blacktriangle , 0.5 Hz; —, laminar theory (Uchida 1956); - - -, present numerical calculations.

performed at very low (transitional) Reynolds number, did not reveal significant departure from laminar-like response. The present experiments have very clearly demonstrated that the response of the turbulent flow to imposed external unsteadiness is not laminar-like. This is true over the range of frequencies of the imposed unsteadiness studied in the present experiments.

In view of statements made above, it is interesting to compare the present experimental results with those obtained from the numerical model. The latter results are also shown in figure 1(a). It is obvious that the predictions are closer to the experimental results than to laminar solutions especially with regard to the location of the peak and extent of the turbulent Stokes layer. However, important quantitative differences are observed between the predictions and the experimental results. At the high frequency, the predicted amplitude ratio remains practically unity in the central region. While this is in agreement with the experiment, it is seen that, near the wall, the measured magnitude of the amplitude overshoot is much larger than that predicted. This again indicates that, in the core region, where the flow is nearly 'frozen' at some mean state, and where the inertia term is very much larger than the shear term, the quasi-steady turbulence model gives satisfactory results. Near the wall, where these conditions are not satisfied, the quasi-steady model works poorly. At lower frequency the experimental results exhibit a mild overshoot followed by smooth decrease to the centreline value. The calculation predicts practically no overshoot and deviates significantly from experiment near the centreline. Similar discrepancy exists near the wall but is not very clearly seen in the figure. This indicates that the quasi-steady turbulence model is not adequate to describe the unsteady turbulent flow in this case.

The phase-angle data are shown in figure 1(b). Also shown in this figure are the results from laminar theory at the same frequencies (or the same Stokes number $\Omega = (\omega D/8\nu)^{1/2}$) as well as the results of the present numerical calculations. It is seen

that, in laminar flow, the velocity near the wall or the wall shear stress (as a limiting case) leads by nearly 45° the cross-sectional-average velocity at both the frequencies. However, both experiments and calculations in turbulent flow indicate very clearly that the phase lead is very much smaller than this. This confirms again that laminar and turbulent flows respond very differently to imposed periodicity and that Stokes number is not a relevant parameter to characterize adequately turbulent periodic pipe flow. Both experiments indicate that the local velocity leads the cross-sectional-average velocity and this lead increases continuously with radius reaching a maximum value at a short distance from the wall. After this, the measured phase lead (surprisingly) seems to decrease. This trend is seen particularly clearly at 0.5 Hz, in the velocity measurements close to the wall. The measured phase angle of the wall shear stress in each of the experiments is shown in figure 1(b) by filled symbols. These results show that (the fundamental component of) the wall shear stress, in fact, lags behind the cross-sectional average velocity by about 8° at the high frequency of 3.6 Hz. However, a reference to figure 10(a) of Part 1 shows that the maximum wall shear stress occurs about 8° ahead of the maximum in $\langle U_m \rangle$. This point is also shown in figure 1(b) by a filled circle with a flag. The difference between the two results is due to the kink in the distribution of $\langle \tau_w \rangle$. In any case, both the values of phase shift are within $\pm 10^\circ$ around 0 and are consistent with the trend exhibited by the velocity data. This result has been confirmed by repeating the wall-shear-stress measurements several times. At 0.5 Hz, the measured phase lead of the wall shear stress is seen to be very nearly zero, which is also consistent with the trend shown by the velocity data near the wall. There has been a considerable controversy among research workers concerning the phase-angle distribution near the wall in turbulent boundary layers and pipe flows. The present measurements made by using two completely independent instrumentation and obtained from independent experiments indicate, albeit within some uncertainty range, that the magnitude of the phase lead/lag near the wall is very small in turbulent shear flows even at high oscillation frequencies. The present data are also in agreement with the earlier data of Ramaprian & Tu (1980). There are no other direct wall-shear-stress measurements in unsteady pipe flow reported in the literature. The validity of those which have been reported depend on the existence of the universal log law in unsteady flows (which was shown in Part 1 to be not true). Some wall-shear-stress measurements obtained using a flush-mounted gauge were reported by Simpson, Shivaprasad & Chew (1981) for unsteady boundary layers. These seem to support qualitatively the existence of a maximum close to the wall in the distribution of the phase angle across the shear flow. The data of Cousteix, Houdeville & Javelle (1981) (again for boundary layers) obtained via the assumption of a universal log law also seem to indicate such a distribution.

Predictions of the present numerical calculations are again seen to be closer to the experimental results than are the results from laminar theory. For example, the turbulence model employed gives nearly correct values for the velocity phase lead over most of the pipe at 3.6 Hz. The predicted phase angle increases monotonically towards the wall and does not show a maximum. However, the positive phase angle of about 18° predicted for the wall shear stress is very much lower than the laminar value of nearly 45° . At 0.5 Hz, the predictions are in some error across the entire pipe. Again no maximum phase lead near the wall is predicted. The predicted phase lead of the wall stress is in error by a few degrees only, while the laminar theory still predicts about 45° for the phase lead. The general conclusion that can be drawn from these comparisons is that the present quasi-steady turbulence model captures the

general features of the flow but fails to follow the changes in flow with sufficient accuracy except when the flow itself behaves as 'frozen'.

3.1.2. *Turbulence intensity*

The results for the amplitude and phase of the ensemble-averaged turbulence intensities as defined in (4) are shown in figure 2. In figure 2(a) the absolute amplitude of turbulence intensity is normalized with the time-mean value of cross-sectional-average velocity. At high frequency, the amplitude in the core region is small because of the frozen structure, as discussed earlier. Near the wall, the amplitude is rather high compared with that of quasi-steady flow experiments. Because of the experimental uncertainty in the measurement of the turbulence intensity, the quasi-steady amplitude distribution shows some distortion, especially at low modulation amplitudes, but is still acceptable for comparison. At the lower frequency of 0.5 Hz with a discharge amplitude of 64 %, the amplitude of the turbulence intensity seems to be higher throughout the pipe than that obtained in quasi-steady flow of similar discharge amplitude.

The phase shift of turbulence intensity with respect to the peak of cross-sectional-average velocity is shown in figure 2(b). Both the experiments indicate a phase lag of the turbulence intensity across most of the pipe. There is, however, a tendency for the turbulence intensity to become in phase with the cross-sectional-average velocity in the vicinity of the wall. At higher frequency, the phase lag is higher than that at the lower frequency except at the central region ($\eta \gtrsim 0.3$), where, at high frequency, the turbulence intensity u'_p is frozen and hence the phase angle is not well defined. Note that the phase shift would be zero everywhere in the quasi-steady flow. No maximum or sign reversal is observed in the phase-angle distribution, in contrast to the case of the velocity. Also, there is a very large phase shift between the ensemble velocity $\langle U_m \rangle$ and the turbulence intensity u'_p over most of the pipe. Thus the mean flow and turbulence structure are decoupled from each other. This can explain why quasi-steady models that relate the turbulence structure to the instantaneous local velocity gradient cannot be expected to work well in this region. In the same figures, the predicted phase-angle distributions of twice the turbulent kinetic energy ($\langle q^2 \rangle = u_p'^2 + v_p'^2 + w_p'^2$) are also plotted for comparison. It is seen that the trend is qualitatively predicted. Quantitative difference, however, exists at both the frequencies. Rigorous comparisons, however, cannot be made since the relation between u'_p and $\langle q^2 \rangle$ is not well established in unsteady flow.

3.1.3. *Reynolds shear stress* $-\langle uv \rangle$

As discussed in Part 1, the prediction of Reynolds shear stress $-\langle uv \rangle$ fails completely at high frequency. This can be clearly seen from figure 3 showing amplitude and phase relations of the shear stress. In this figure, the amplitude is normalized by the amplitude of the ensemble wall shear stress. It is seen that, at 3.6 Hz, the amplitude of $-\langle uv \rangle$ reaches, at one location, a value as high as 3 times that of the wall shear stress. At this high frequency, the phase lead of $-\langle uv \rangle$ ranges from 270° to 300° (or a lag of 90° – 60°) everywhere in the whole section. This is completely different from either the trend predicted or the experimental results for turbulence intensity and ensemble-averaged velocity. This implies a complete breakdown of equilibrium in the turbulence structure.

At the lower frequency of 0.5 Hz the experiments show qualitative agreement with the predicted values. (It should be noted that near the centreline, where the shear stress is nearly zero, there is a considerable uncertainty in the phase-angle determi-

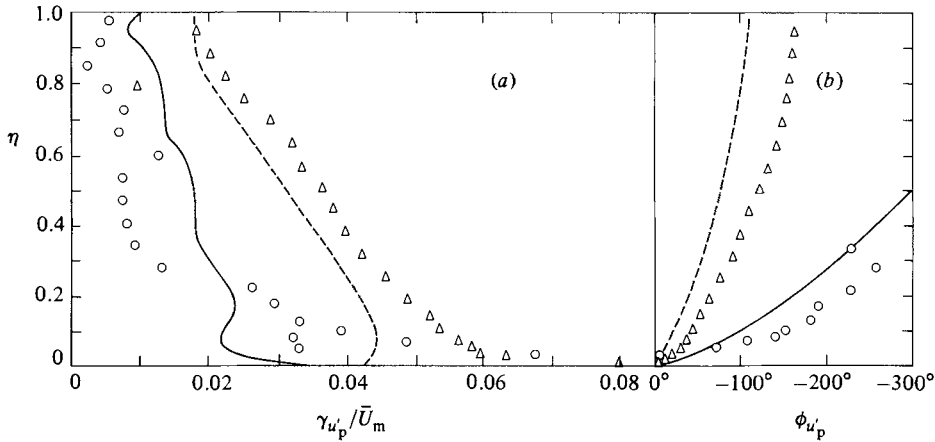


FIGURE 2. Amplitude and phase of the longitudinal turbulence intensity u'_p : (a) Amplitude: \circ , 3.6 Hz; \triangle , 0.5 Hz; ---, quasi-steady flow with $\gamma_{U_m} \approx 0.60$; —, quasi-steady flow with $\gamma_{U_m} \approx 0.15$. (b) Phase: \circ , 3.6 Hz; \triangle , 0.5 Hz; —, numerical prediction for $\langle q^2 \rangle$ at 3.6 Hz; ---, numerical prediction for $\langle q^2 \rangle$ at 0.5 Hz.

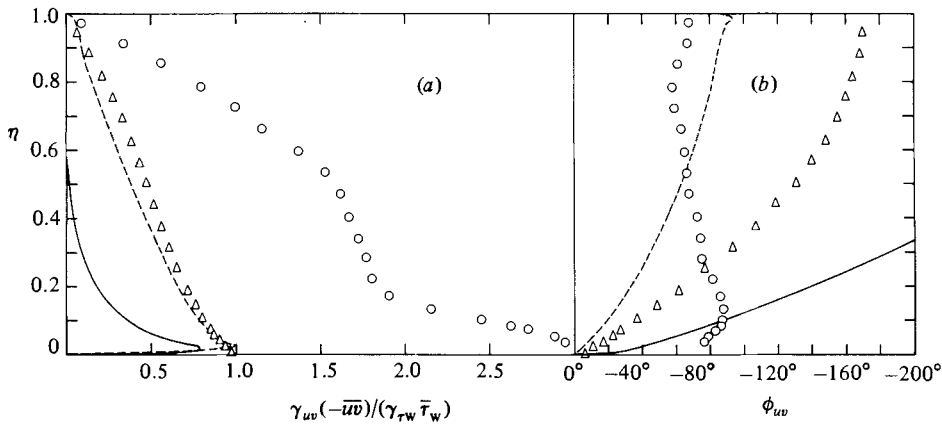


FIGURE 3. Amplitude and phase of the Reynolds shear stress $-\langle uv \rangle$: (a) amplitude; (b) phase; \circ , 3.6 Hz; \triangle , 0.5 Hz; —, prediction at 3.6 Hz; ---, prediction at 0.5 Hz.

nation.) It is interesting to see that, at this frequency, there is a strong resemblance between the turbulence intensity u'_p and Reynolds shear stress $\langle uv \rangle$ with respect to the distributions of phase and amplitude. Therefore, even though the two turbulence quantities are completely out of phase with the velocity, they are mutually in step with each other. This implies the existence of some kind of equilibrium in the turbulent structure of the flow even though the flow is not quasi-steady, and even though the instantaneous ensemble-averaged turbulent structure is not related to the instantaneous ensemble-averaged velocity. Again, comparisons with numerical predictions are shown in figure 3. It is seen that, except for the amplitude at 0.5 Hz, the dynamics of the ensemble-averaged Reynolds shear stress is predicted very poorly.

3.2. Effect of oscillation frequency on the amplitude and phase angle – results of series 3 experiments

The above results showed details of amplitude and phase-angle distributions of various properties of the flow at two oscillation frequencies, modulation of discharge

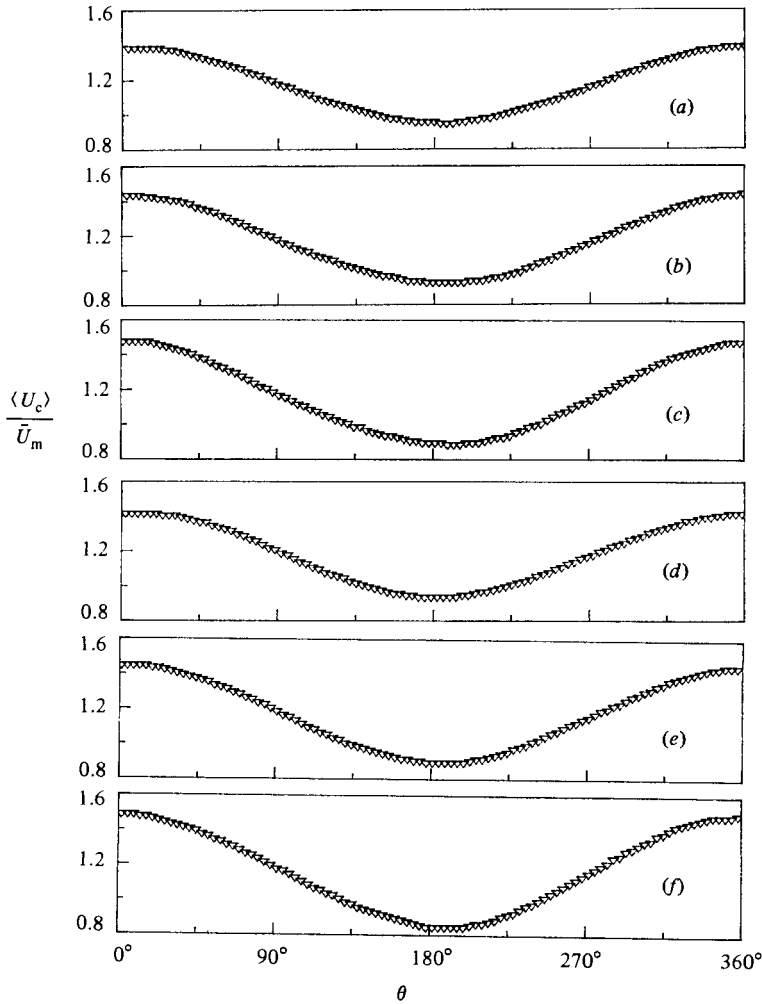


FIGURE 4. Ensemble-averaged velocity variation at centreline in the experiments of series 3: (a) 3.0 Hz; (b) 2.5 Hz; (c) 2.0 Hz; (d) 1.5 Hz; (e) 1.0 Hz; (f) 0.5 Hz.

being 15% in one case and 64% in the other. As mentioned earlier, the third series of experiments were conducted at six oscillation frequencies to study the influence of oscillation frequency on the flow structure, maintaining all other conditions nearly constant. The ensemble-averaged velocities and longitudinal turbulence intensities at the centreline are shown in figures 4 and 5 for these 6 frequencies. It should be noted that all the phase angles are now referred to the maximum of the centreline velocity $\langle U_c \rangle$ instead of to the maximum of the cross-sectional-averaged velocity $\langle U_m \rangle$ since the latter was not measured in this series of experiments.

Figure 4 shows that the centreline velocity distributions at off-design frequencies are slightly distorted and have slight differences in amplitude (again note that these amplitudes should also correspond approximately to the amplitude of the cross-sectional-averaged velocity). These are not considered to be significant for the purpose of the present discussions. It is seen from figure 5 that the ensemble-averaged turbulent intensity u'_{pc} at the centreline exhibits clearly a cyclic variation at the lowest frequency (0.5 Hz), and the modulation of this variation is attenuated and becomes practically zero as the frequency is increased. The relative amplitude of

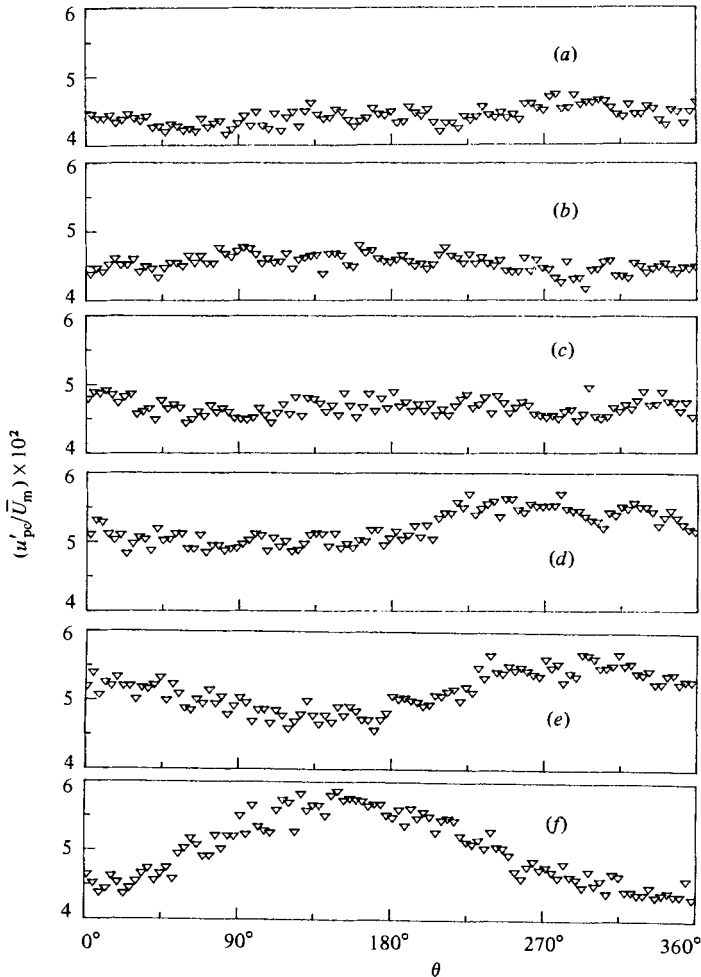


FIGURE 5. Ensemble-averaged turbulence intensity at the centreline in the experiments of series 3: (a) 3.0 Hz; (b) 2.5 Hz; (c) 2.0 Hz; (d) 1.5 Hz; (e) 1.0 Hz; (f) 0.5 Hz.

the turbulence intensity and its time-mean value are shown as a function of the imposed frequency in figure 6. It can be seen clearly that the relative amplitude $\gamma_{u'_{pc}}$ becomes smaller as the frequency is increased, from $\gamma_{u'_{pc}} = 13\%$ at $f_{os} = 0.5$ Hz to 4% at $f_{os} = 2.0$ Hz. The corresponding value for the quasi-steady flow (zero frequency) with similar amplitude was obtained from the steady-flow experiments. This value (of about 21%) is also shown in the figure. Considering the experimental uncertainties in the measurement of u'_p (shown by the vertical bar in the figure), it can be concluded that the relative amplitude goes nearly to zero beyond a frequency of about 2 Hz. It is also interesting to see that the time-mean turbulent intensity u'_c at the centreline reaches a peak value in the frequency range 0.5–1.5 Hz and then decreases as frequency increases, and eventually attains a value approximately equal to that of the quasi-steady flow. The intensity of turbulence measured at 0.5 Hz and 64% amplitude is also shown in this figure for comparison. It is seen that the effect of the amplitude γ_{U_m} alone (largely a quasi-steady Reynolds-number effect) is not very significant. In any case, it is not sufficiently larger than the experimental uncertainty indicated by the vertical bar, to require further comments.

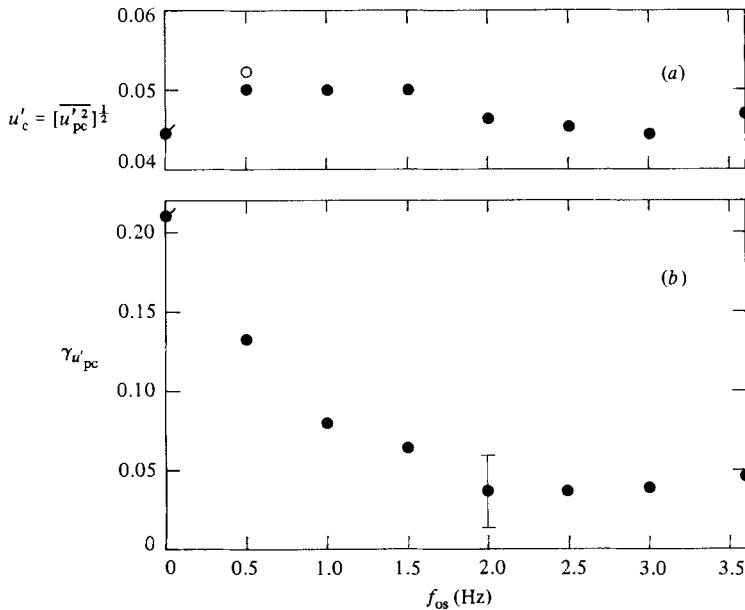


FIGURE 6. Time-mean value and amplitude of the longitudinal turbulence intensity u'_{pc} at the centreline in the experiments of series 3: (a) time-mean value; (b) amplitude. Symbols with flag represent data for quasi-steady flow with $\gamma_{U_m} = 30\%$, while the open circle represents unsteady flow at 0.5 Hz and $\gamma_{U_m} = 64\%$.

The wall-shear-stress measurements at the six different frequencies are shown in figure 7. The distributions are seen to be reasonably smooth at the lower frequencies. At 3.0 Hz, some mild kinks begin to appear. These distortions are, however, not as strong as those observed at 3.6 Hz in the earlier series of experiments. The time-mean wall shear stress and its relative amplitude are shown in figure 8. It is seen that the relative amplitude decreases as frequency increases from zero to 3.0 Hz. But the rate of decrease with frequency is small and, unlike the flow at centreline, does not go to zero even at 3.0 Hz. In other words, the flow in the wall region still responds to the flow oscillations, though less 'vigorously' than at low frequencies. However, the time-mean wall shear stress does not show a consistent trend as the frequency is increased. The observed increase in time-mean wall shear stress at 3.6 Hz is confirmed by this series of experiments also. It is also seen that at 0.5 Hz, the time-mean wall shear stress at 64% amplitude (○) is larger than that at 30% amplitude of modulation (●). Again, this is to be expected from the quasi-steady results discussed in Part 1.

The phase shifts of the centreline turbulence intensity and wall shear stress are shown in figure 9. It is seen that the wall shear stress leads the centreline velocity by a small angle. This angle increases to only about 10° at 3 Hz. The results for 3.6 Hz will be consistent with this trend if the phase angle corresponding to the maximum value of $\langle \tau_w \rangle$ is used. On the other hand, the use of the phase angle for the fundamental Fourier component appears to depart from the trend. This is because of the kink in the distribution of $\langle \tau_w \rangle$ already referred to. Both values are shown in figure 9. The apparent non-monotonic trend observed at 0.5 Hz is due to the phase shift of about -10° of the centreline velocity itself, with respect to the cross-sectional-average velocity, which will decrease to (nearly) zero at higher frequencies. It is also interesting to see that the phase shift of the wall shear stress at 0.5 Hz is

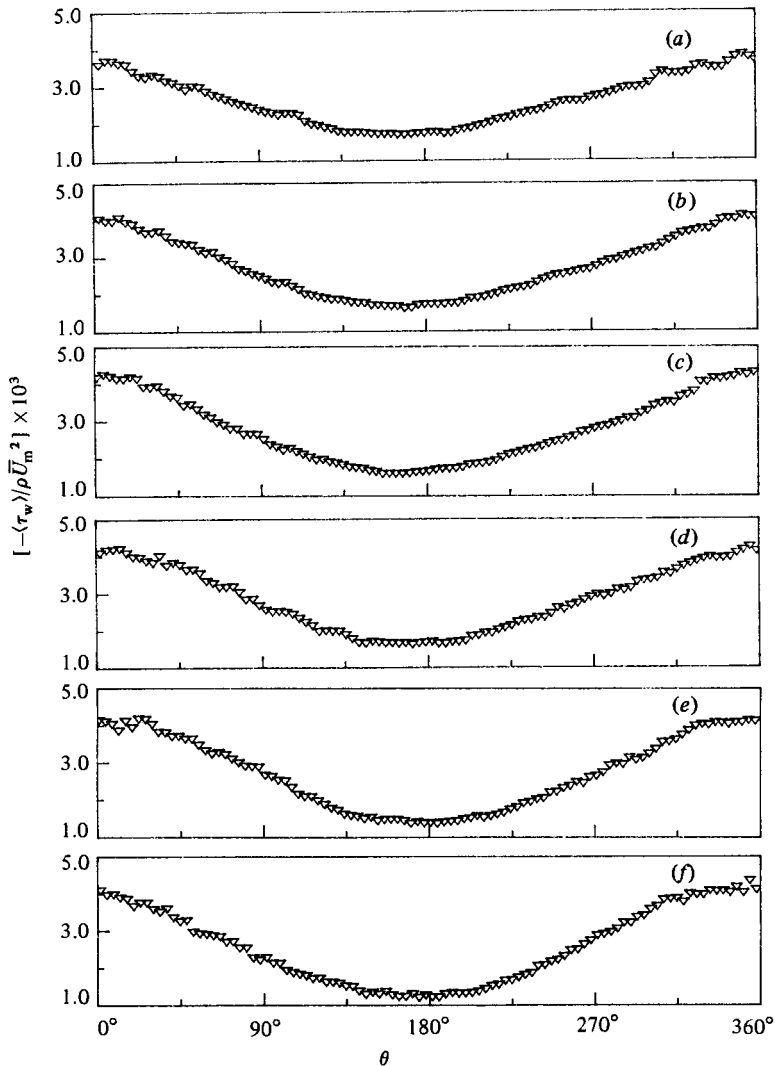


FIGURE 7. Ensemble-averaged wall-shear-stress variation in the experiments of series 3: (a) 3.0 Hz; (b) 2.5 Hz; (c) 2.0 Hz; (d) 1.5 Hz; (e) 1.0 Hz; (f) 0.5 Hz.

the same at 30% as well as 64% amplitude. The phase shift of the turbulence intensity u'_{pc} at the centreline relative to the centreline velocity is shown in the bottom part of figure 9. It is seen that the turbulence intensity lags behind the velocity and the phase lag increases drastically (0° to 360°) in the frequency interval zero to about 1.0 Hz. At 2 Hz and beyond, the turbulence intensity is nearly frozen and hence phase shift cannot be accurately measured. It is also observed from the results at 0.5 Hz that amplitude of discharge modulation has no effect on the phase lag of u'_{pc} .

The present results can be compared with the lag distribution implied by the measurements of Mizushima, Maruyama & Hirasawa (1975). They obtained, from autocorrelation measurements, the timelag Δt_c between the instants of peak turbulence intensity at the centreline and at (or near) the wall. They showed that the dimensionless time lag $\Delta t_c \bar{U}_m/D$ (phase lag) at the centreline in the unsteady flow approximately equals the dimensionless time-mean bursting period $\bar{T}_b \bar{U}_m/D$ in

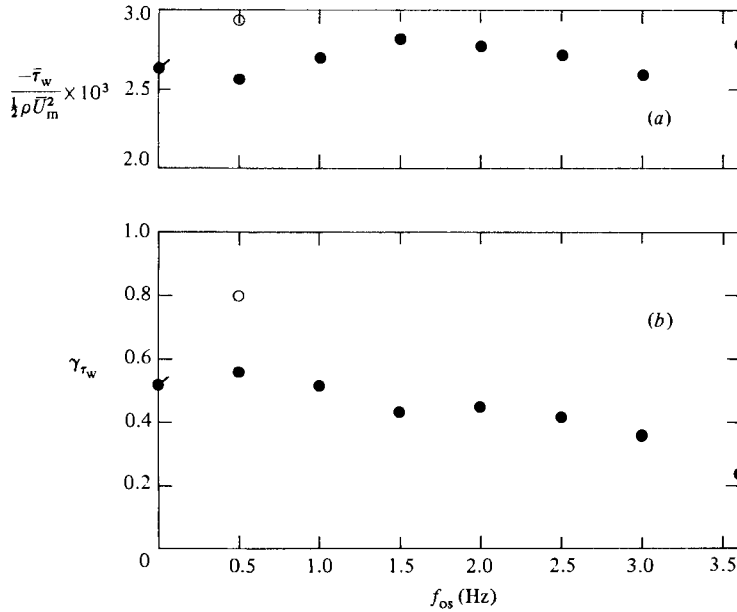


FIGURE 8. Time-mean value and relative amplitude of the wall shear stress in the experiments of series 3. Flagged symbols and open circle as in figure 6.

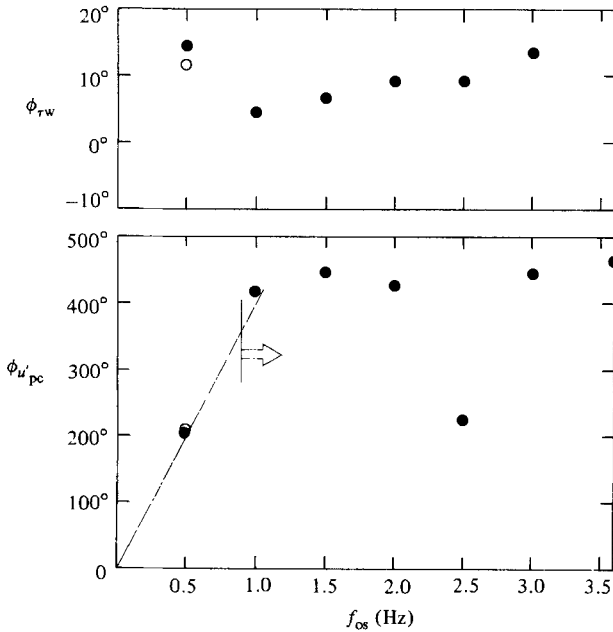


FIGURE 9. Phase of u'_{pc} and $\langle \tau_w \rangle$ in the experiments of series 3. Note that these phase angles shown in this figure are relative to the maximum of $\langle U_c \rangle$. Open symbols as in figure 6; half-filled circles correspond to the τ_w data at 3.6 Hz and $\gamma_{U_m} = 15\%$. \bullet , fundamental frequency; \blacklozenge , maximum value of $\langle \tau_w \rangle$. —, equation (8); arrow denotes regime in which turbulence structure is frozen at the centreline.

steady flow and is independent of the oscillation frequency. They found from these experiments that, at a Reynolds number of 50000,

$$\frac{\Delta t_c \bar{U}_m}{D} = \frac{\bar{T}_b \bar{U}_m}{D} \approx 20. \quad (7)$$

By writing $\Delta t_c = \phi_{u'_{pc}} T/2\pi$, one gets from (7)

$$\phi_{u'_{pc}} = 40\pi D f_{os} / \bar{U}_m. \quad (8)$$

The straight line obtained by substituting in (8) the experimental values of $D = 5$ cm and $\bar{U}_m = 1$ m/s is also shown in figure 9. It is seen to agree well with the experimental data. The arrow in this figure shows the frequency beyond which the turbulence structure at the centreline can be expected to be frozen because the disturbance from the wall cannot reach the centreline within one oscillation period T . This requirement according to (7) is given by

$$T\bar{U}_m/D \lesssim 20,$$

or equivalently

$$f_{os} \gtrsim \bar{U}_m/20D \approx 0.9 \text{ Hz}, \quad (9)$$

using again the experimental values of \bar{U}_m and D . The estimated value seems to be in agreement with observation as seen from figure 9.

3.3. Energy spectra of u'

Figure 10(a) shows spectral density distributions of u'^2 at two typical locations, namely $\eta = 0.08$ and $\eta = 0.64$ for unsteady flow at $f_{os} = 3.6$ Hz (spectrum 1) and for steady flow (spectrum 2). Also shown for each location is the spectrum (3) of $(\bar{U}_p + u)^2$, corresponding to the total velocity fluctuation before removing the deterministic part via ensemble averaging. These are all non-dimensional spectra in the wavenumber domain, with the non-dimensional spectral density $G(KR)$ being defined in the usual way as follows:

$$G(KR) = \frac{G_f(f) \bar{U}}{2\pi R u'^2} \quad \text{for spectra 1 and 2}, \quad (10)$$

$$G(KR) = \frac{G_f(f) \bar{U}}{2\pi R (\bar{U}_p + u)^2} \quad \text{for spectrum 3}, \quad (11)$$

where $G_f(f)$ is the spectral density function and K is the wavenumber given by

$$K = \frac{2\pi f}{\bar{U}}, \quad (12)$$

f being the frequency. With the above definitions, we have

$$\int_0^\infty G(KR) d(KR) = 1. \quad (13)$$

Note that the spectrum 3 obtained without removing the periodic component exhibits a peak at the wavenumber corresponding to the oscillation frequency. Referring first to the spectra at $\eta = 0.08$, one can see from a comparison of the spectra 1 and 2 that in the unsteady flow there is a reduction (of about 25%) in the spectral density at the low-wavenumber end. Since the area under each spectrum has to be unity, the attenuation of the large eddies must be compensated by an increase in the energy content in the middle and high wavenumber range, as can be seen from figure 10(a). Figure 10(a) also shows that, as η increases to 0.64, the attenuation of the low wavenumber end becomes more significant. This decrease is accompanied by an increase

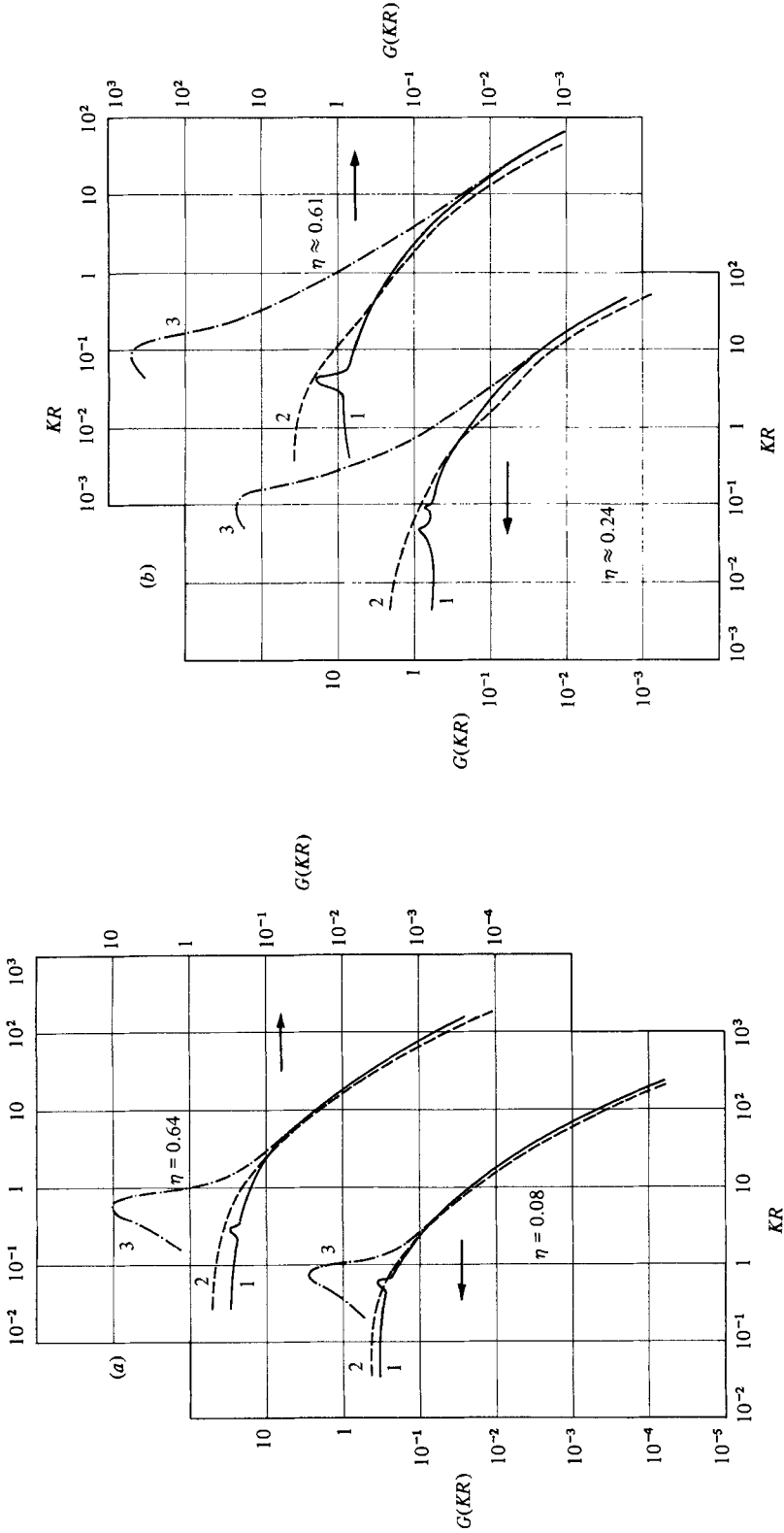


FIGURE 10. (a) Spectra of u'^2 at $f_{os} = 3.6$ Hz compared with corresponding spectra in steady flow. Bottom figure refers to $\eta = 0.08$; top figure refers to $\eta = 0.64$. Curve 3 refers to $(U_p + u)^2$. (b) Spectra of u'^2 at $f_{os} = 0.5$ Hz compared with corresponding spectra in steady flow. Bottom figure refers to $\eta \approx 0.24$; top figure refers to $\eta \approx 0.61$. Curve 3 refers to $(U_p + u)^2$.

in the energy content of the higher wavenumbers. A careful observation of the two spectra in this figure reveals that imposed oscillations tend to attenuate eddy scales larger than that corresponding to the oscillation frequency (peak of spectrum 3), this energy being transferred to larger wavenumbers as distance from the wall increases.

Figure 10(b) shows typical spectra obtained in periodic flow at 0.5 Hz and at the same locations in steady flow. The different spectra are labelled in these figures in the same way as in figure 10(a). It is seen that the same trends present at the higher oscillation frequency are present at this frequency also. In fact, the attenuation of wavenumbers smaller than that corresponding to the oscillation frequency is more pronounced in this case than at the higher oscillation frequency. The attenuation is stronger as the distance from the wall increases. The corresponding amplification of the high-wavenumber scales is also stronger than at the higher frequency of oscillation. The spectra of u'^2 are seen to exhibit periodicity around a wavenumber of 0.4 corresponding approximately to half the oscillation frequency. This is perhaps due to the fact that, at 0.5 Hz, the turbulent intensity was not frozen but varied significantly during the cycle (see figure 12(b) of Part 1). The peaks are not very pronounced in the spectra for 3.6 Hz.

3.4. Turbulent-energy production

Figure 11 shows the variation of the rate of turbulent-energy production during the oscillation cycle at two typical locations in the pipe. Also shown is the rate of change of $\frac{3}{2}u_p'^2$ (which can be assumed to be representative of the rate of change of turbulent kinetic energy). First, with reference to figure 11(a) corresponding to 0.5 Hz, it is seen that at $\eta \approx 0.2$ the turbulent energy increases ($\partial\langle u_p' \rangle / \partial t > 0$) during the period $0^\circ < \theta \lesssim 75^\circ$, and decreases to its minimum value at about 180° . It is then almost frozen in that state till about 270° before beginning to increase again. It is also observed that the maximum rate of production occurs during the retardation, as is to be expected. However, production lags behind velocity by about 45° . There is very little production during the first half of the acceleration period ($\theta = 180^\circ$ – 270°). Thus, near the wall, production is not in step with the mean flow field, and the turbulent energy is not in step with production. The upper part of figure 11(a) shows the results for the location $\eta \approx 0.5$. It is seen that at this station the rate of production of turbulent energy is very small and is out of phase with the velocity. Further, the turbulent kinetic energy is seen to be frozen at its minimum value over nearly half the cycle, and during this time there is practically no production of turbulence locally. In fact, production is very small, even near the wall, during this period. This steep drop in production is due to a decorrelation between the Reynolds shear stress and the velocity gradient. This indicates that the flow is not quasi-steady, and eddy-viscosity-type models relating the turbulence structure to the local velocity gradient are not entirely realistic. Figure 11(b) shows corresponding results for the oscillation frequency of 3.6 Hz. It is seen that at $\eta \approx 0.2$ the rate of production shows a cyclic variation with maximum at 130° and minimum at 270° . The $\partial\langle u_p'^2 \rangle / \partial t$ term is seen to be randomly scattered around zero, indicating a frozen turbulence structure. An important thing to note is that, at this high frequency, production is not zero at $\eta \approx 0.5$ except for a short interval of time (around $\theta = 270^\circ$), unlike in the case of the 0.5 Hz experiment, in which production of turbulent energy remained practically zero for nearly half the cycle, at this same location. To sum up, it appears that, at the high frequency, turbulent production undergoes variations during a cycle (especially near the wall), but with a phase lag of more than 90° with respect to the velocity, while the turbulent kinetic energy seems to be practically frozen over most of the pipe.

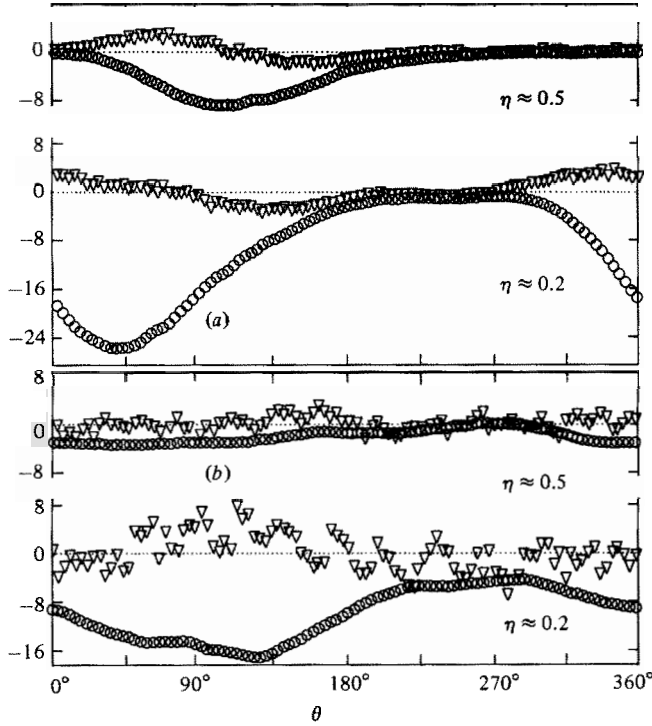


FIGURE 11. Variation of the ensemble-averaged rate of turbulent energy production $P = -\langle uv \rangle (\partial \langle U \rangle / \partial r)$ and the rate of increase of ensemble-averaged turbulent kinetic energy $\langle \partial k / \partial t \rangle$ (assumed to be proportional to $3\partial u_p^2 / \partial t$): (a) 0.5 Hz; (b) 3.6 Hz; \circ , $-PD/2\bar{U}_*^3$; ∇ , $3(\partial u_p^2 / \partial t) D/2\bar{U}_*^3$.

Thus the turbulent kinetic energy, turbulent production and velocity field are decoupled from one another.

4. Characteristic parameter for periodic turbulent pipe flow

4.1. The 'turbulent Stokes number'

It is known that, in the case of the unsteady laminar pipe flow, the Stokes number Ω defined as $\frac{1}{2}D(\omega/2\nu)^{\frac{1}{2}}$ is the only important parameter characterizing the flow. This number can also be interpreted as the ratio of two characteristic lengthscales, namely the pipe radius and the viscous length $(2\nu/\omega)^{\frac{1}{2}}$. The latter is a measure of the radial distance from the wall toward the centre that any disturbance at the wall can reach by means of diffusion within one period of the cycle. In an analogous manner, one may use a modified Stokes number for turbulent flow by replacing the kinematic viscosity ν in laminar flow by some eddy viscosity ν_t in turbulent flow. Then the diffusion distance y in time t is given by

$$y = (\nu_t t)^{\frac{1}{2}}, \quad (14)$$

or

$$t = y^2 / \nu_t. \quad (15)$$

Differentiating (15), one gets

$$\frac{dt}{dy} = \frac{2y}{\nu_t} - \frac{y^2}{\nu_t^2} \frac{d\nu_t}{dy}. \quad (16)$$

In order to make a qualitative analysis, let us assume a simple time-independent distribution of ν_t as follows:

$$\nu_t = \kappa \bar{U}_* y \quad (y \leq y_0; \text{inner layer}), \quad (17)$$

$$= \frac{1}{2} c \bar{U}_* D \quad (y_0 \leq y \leq \frac{1}{2} D; \text{outer layer}), \quad (18)$$

where \bar{U}_* is the time-mean shear velocity, κ and c are constants (κ being the well-known von Kármán constant, assumed to be equal to 0.4), and y_0 is determined from the matching condition

$$\kappa \bar{U}_* y_0 = \frac{1}{2} c \bar{U}_* D, \quad (19)$$

as

$$y_0 = \frac{c D}{\kappa 2}. \quad (20)$$

From (16)–(18), and integrating from the wall, one gets, for the inner layer ($y \leq y_0$),

$$t = \frac{y}{\kappa \bar{U}_*}, \quad (21)$$

and integrating from y_0 outwards one gets

$$y^2 - y_0^2 = \frac{1}{2} c \bar{U}_* D (t - t_0), \quad (22)$$

where $t_0 = y_0 / \kappa \bar{U}_*$ is the time of diffusion up to $y = y_0$. From (22), one finally obtains the total time of diffusion up to any point y as

$$t = \frac{2y^2}{c \bar{U}_* D} = \frac{y^2}{\nu_{t \text{ outer}}}. \quad (23)$$

In other words, the diffusion time (in the outer layer) can be computed using the constant eddy viscosity $\nu_{t \text{ outer}}$ in place of the laminar viscosity ν . Since $\nu_{t \text{ outer}} \gg \nu$, the diffusion time in turbulent flow is very much smaller – usually 2–3 orders of magnitude smaller – than that in laminar flow. Rearrangement of (23) gives

$$\frac{\bar{U}_* t}{D} = \frac{1}{2c} \eta^2. \quad (24)$$

Also, the total time

$$\Delta t_c = \frac{D}{2\bar{U}_*} \frac{1}{c}. \quad (25)$$

If c is taken as 0.07 from Hinze (1959), one obtains

$$\Delta t_c = 7.15 D / \bar{U}_*. \quad (26)$$

Hence, in a periodic flow of circular frequency $\omega = 2\pi f_{\text{os}}$, the disturbance can diffuse from the wall to the centreline within one oscillation period $2\pi/\omega$, if $\Delta t_c \leq 2\pi/\omega$, which gives the condition

$$\frac{\omega D}{\bar{U}_*} \lesssim 0.88 \approx O(1). \quad (27)$$

Thus $\omega D / \bar{U}_*$ is the equivalent turbulent Stokes number to characterize periodic turbulent flow. Since

$$\frac{\omega D}{\bar{U}_*} = \frac{\omega D^2}{8\nu} \frac{8\nu}{\bar{U}_* D} = \frac{8\Omega^2}{\bar{U}_* D / \nu}, \quad (28)$$

the turbulent Stokes number is very much smaller than the conventional (laminar) Stokes number for the same frequency, and the ratio of turbulent to laminar Stokes

number decreases as the Reynolds number $\bar{U}_* D/\nu$ increases. Hence what may be regarded as a large oscillation frequency in laminar flow ($\Omega \gg 1$) may not be large or may even be regarded as low frequency in turbulent flow, depending on the value of $\omega D/\bar{U}_*$. This explains the drastic differences between the behaviour of laminar and turbulent periodic flows at the same oscillation frequency (see figure 1). In the same way, it is now clear that categorizing turbulent pipe flows by the so-called Strouhal number $\omega D/\bar{U}_m$ is also not very useful, since $\omega D/\bar{U}_m = (\omega D/\bar{U}_*) \bar{U}_*/\bar{U}_m$, and hence the behaviour of the flow will depend on the Reynolds number also.

The above discussion indicated the extent to which disturbances from the wall can spread in the turbulent periodic flow. For instance, at $\omega D/\bar{U}_* \ll 1$, the unsteady effects would diffuse throughout the pipe, with the result that the ensemble-averaged velocity at all points in the pipe will suffer amplitude variation and phase shift relative to the cross-sectional-averaged flow. At $\omega D/\bar{U}_* \gg 1$, these effects would be confined to a very thin layer of thickness of the order of \bar{U}_*/ω beyond which the flow would oscillate like a solid body. In fact, a careful study of figure 1 shows that the thickness of the turbulent Stokes layer (say location of the peak amplitude) is given approximately by \bar{U}_*/ω .

4.2. *The use of the turbulent Stokes number in the classification of periodic turbulent shear flows*

The turbulent Stokes number is a measure of the relative distance from the wall up to which the unsteady effects will penetrate. No consideration was given in its derivation to the interaction of the turbulence structure and imposed oscillations. In fact, in the derivation of the Stokes parameter, $\langle U_* \rangle$ is assumed to be approximated by its average value \bar{U}_* , which is regarded as known. Whether the turbulent structure is affected by unsteadiness or not depends on whether the oscillation frequency ω (or f_{os}) interacts with a characteristic frequency of turbulence f_t . The characteristic frequency that can be used for this purpose is the so-called 'turbulent bursting frequency'. Considerable information (though conflicting) is available on this frequency in turbulent boundary layers. However, as far as the authors are aware, the only such data reported on pipe flows are those of Mizushima, Maruyama & Shiozaki (1973). They measured not only the mean bursting period \bar{T}_b but also the histogram of the intervals between the bursts. They found that, in the Reynolds-number range 10^3 – 10^5 , the lower and upper ends of the histogram T_{bL} and T_{bU} , as well as the mean burst period \bar{T}_b , depend on Reynolds number. The following approximate relations can be obtained from their measurements (see Ramaprian & Tu 1982):

$$\omega_{bL} D/\bar{U}_* \approx 166 Re^{-0.54}, \quad (29)$$

$$\bar{\omega}_b D/\bar{U}_* \approx 1.58 Re^{\frac{1}{2}}, \quad (30)$$

$$\omega_{bU} D/\bar{U}_* \approx 31 Re^{0.125} [10^{-(3.32-0.667 \log Re)}], \quad (31)$$

where ω is the circular frequency $2\pi/T$ in each case.

We can now combine the information on the interaction between unsteadiness and turbulent structure with the diffusion information obtained earlier in §4.1 to classify the periodic flow into several regimes.

These results are shown in figure 12. In this figure, the three lines corresponding to (29)–(31) are shown. In addition, a fourth line (chain-dotted) is also shown in this figure. This line is obtained from Mizushima *et al.* (1975) and corresponds to the oscillation frequency at which the modulation amplitude γ_{U_m} is attenuated by 5% relative to the quasi-steady value. This line can be arbitrarily defined as the 'quasi-steady' line.

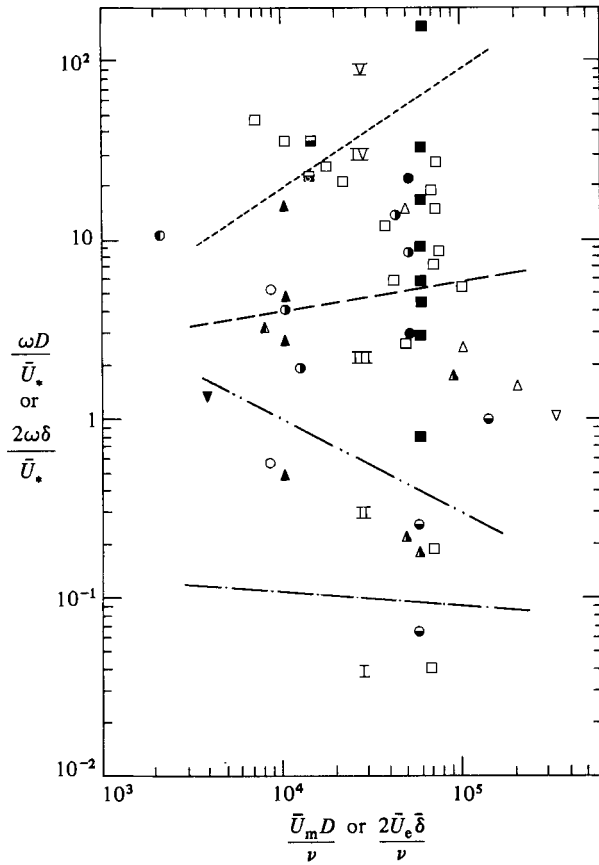


FIGURE 12. Classification of unsteady turbulent shear flows: \odot , Ramaprian & Tu (1980); \bullet , present experiments; \blacktriangle , Mizushima *et al.* (1973, 1975); \blacktriangledown , Gerard (1971); \circ , Binder & Kueny (1981); \ominus , Kita, Adachi & Hirose (1979); \odot , Cousteix *et al.* (1981); \triangle , Kirmse (1980); ∇ , Simpson, Shivaprasad & Chew (1981); \square , Ohmi *et al.* (1976); \blacksquare , Karlsson (1959); \blacksquare , Acharya & Reynolds; \blacktriangle , Schultz-Grunow (1940); \blacktriangle , Kobashi & Hayakawa (1981); $-\cdot-$, quasi-steady line from Mizushima *et al.* (1975). $-\cdot-\cdot-$, ω_{bL} (equation (29)); $-----$, ω_b (equation (30)); $\cdot\cdot\cdot\cdot\cdot$, ω_{bu} (equation (31)). Note that, in the case of boundary-layer data, time-mean freestream velocity \bar{U}_e and time-mean boundary-layer thickness δ are used as reference velocity and lengthscales in place of \bar{U}_m and $\frac{1}{2}D$ respectively.

It is interesting to note from figure 12 that the lower limit of the burst histogram corresponds to a value of $\omega_{bL}D/\bar{U}_*$ of the order 1 (In fact for $Re > 10^4$, $\omega_{bL}D/\bar{U}_*$ is seen to be less than 1). Thus, when the oscillation frequency is such that $\omega D/\bar{U}_* \sim 1$, not only does the imposed unsteadiness begin to influence the turbulence structure but, also, this effect can spread across the entire flow. This experimental observation removes the erroneous belief that at oscillation frequencies high enough to interact with turbulence structure the effects are confined to a negligibly thin layer and that flow prediction at such frequencies does not therefore present difficulties from a practical point of view.

We can now proceed to classify the unsteady flow into 5 regimes based on the value of $\omega D/\bar{U}_*$ and the Reynolds number. These five regimes are indicated in figure 12.

Regime I

It is seen from the figure that in this regime $\omega D/\bar{U}_* \lesssim (\omega D/\bar{U}_*)_{\text{quasi-steady}}$, and hence the flow behaves like steady flow. Hence, there will be no amplitude overshoot and no phase lag of the ensemble averaged velocity. Further, since $\omega D/\bar{U}_* \ll \omega_{\text{bL}} D/\bar{U}_*$, turbulent structure is also quasi-steady. Hence a quasi-steady turbulence closure model can describe this flow at all instants. In fact, the ensemble averaged flow can be solved as a succession of steady flows. This regime can be designated as the 'quasi-steady regime'. In this regime $\omega D/\bar{U}_* \lesssim 10^{-1}$.

Regime II

The flow departs from quasi-steady behaviour, the departure increasing with the value of $\omega D/\bar{U}_*$. The effect of oscillation on the ensemble-average velocity field will spread across the entire shear layer. The turbulent structure, however, is not affected since $\omega D/\bar{U}_*$ is still less than $\omega_{\text{bL}} D/\bar{U}_*$. Hence a quasi-steady turbulence model can still be used to predict the flow. However, it is necessary to perform a time-dependent calculation to predict the time history of the flow. Amplitude overshoot and phase lag will be present all across the shear layer in the periodic component of the velocity. The time-mean flow will not be significantly different from that of the quasi-steady flow. This regime may be called the 'low-frequency regime'. In this regime the condition $10^{-1} < \omega D/\bar{U}_* \lesssim 1$ is satisfied at the higher Reynolds numbers.

Regime III

In this regime $\omega_{\text{bL}} D/\bar{U}_* < \omega D/\bar{U}_* < \bar{\omega}_b D/\bar{U}_*$. Hence one can expect to find some interaction between the turbulence structure and the imposed unsteadiness. The interaction will begin from the lower end of the burst frequency histogram and spread to higher frequencies as $\omega D/\bar{U}_*$ increases. This causes the turbulent structure to be affected. This effect spreads across a substantial part of the shear layer. Both the periodic and turbulent structure across a substantial part of the flow will deviate from the quasi-steady flow. The deviation at a given Reynolds number tends to be greater as oscillation frequency increases. Quasi-steady turbulence models will begin to fail and become increasingly unsatisfactory as $\omega D/\bar{U}_*$ increases. The structural equilibrium of turbulence may begin to break down at least during a part of the cycle. The time-mean flow will still be nearly the same as in quasi-steady flow, especially at the lower frequencies. This regime can be called the 'intermediate-frequency regime', and is approximately characterized by $1 \lesssim \omega D/\bar{U}_* < 10$. The present experiment at 0.5 Hz ($\omega D/\bar{U}_* \approx 3$) exemplifies this regime.

Regime IV

The imposed oscillation will interact strongly with the turbulent bursting process at the wall. The effect on the turbulent structure is therefore strong. The time-mean velocity will be affected and can exhibit an inflective profile near the wall. The periodic flow will also be affected but, since $\omega D/\bar{U}_*$ is large in this regime, this effect is confined to a thin region (say, less than 10% of the diameter) beyond which the flow oscillates like a solid mass. The turbulence structure will exhibit total departure from equilibrium. In fact, the turbulence intensity remains practically frozen across the outer part of the shear layer. Quasi-steady turbulence modelling breaks down completely. Yet calculations based on quasi-steady turbulence models still predict the periodic flow in the outer layer reasonably well, since the turbulent shear-stress term is almost negligible compared with the pressure-gradient term at this frequency

in this region. In other words, the periodic flow in the outer region behaves like an inviscid flow. This regime in which $\omega D/\bar{U}_*$ is of the order of 10 can be called the 'high-frequency regime'. The present experiment at 3.6 Hz with $\omega D/\bar{U}_* \approx 20$ falls into this regime.

Regime V

In this region $\omega D/\bar{U}_* > \omega_{bU} D/\bar{U}_*$. This regime can be called the 'rapid-oscillation regime'. $\omega D/\bar{U}_*$ will be typically of the order of 100 in this regime. Hence the interaction between the imposed oscillations and the turbulence structure will be very strong. The effect on the periodic flow will, however, be confined to a very thin layer (of the order of $0.01D$) near the wall. Very little information is presently available on the turbulence structure in this regime.

Many of the recent experiments on periodic pipe and boundary-layer flows are shown in figure 12 in terms of the turbulent Stokes number *vs.* Reynolds number. (In the case of the boundary layer $\frac{1}{2}D$ is replaced by the mean boundary-layer thickness $\bar{\delta}$. Also, the boundary-layer results should be interpreted with caution since the burst information used in the present discussion was obtained from pipe-flow experiments and is at some variance with boundary-layer data.) These experiments can now be discussed in the light of the above classification of unsteady flows. It is seen that most experiments have been performed in regimes III and IV, which are the most important regimes from a practical point of view. The present experiments at 0.5 Hz, and the experiments of Mizushina *et al.* (1973, 1975), Kobashi & Hayakawa (1981) and Cousteix *et al.* (1981) in the 'intermediate-frequency' range, indicate a significant influence of oscillation frequency on the turbulent structure and negligible effect on time-mean flow. The others do not contain detailed information on turbulence. The present experiments have also shown that there is a small effect on the time-mean flow (which is generally hard to detect). There are fewer detailed experiments in the 'high-frequency' range. Since the effects of oscillation are confined to smaller regions and also effects on time-mean velocity and wall shear stress are generally of the order of only 10%, large amplitudes and good experimental accuracy are required to detect these effects. The experiments of Ohmi *et al.* (1976) and Kirmse (1979) do not contain turbulence data. The amplitude of modulation was very small in the experiments of Acharya & Reynolds (1975) and Binder & Kueny (1981). Karlsson's (1959) experiments on boundary layers seem to indicate that the turbulence structure is affected, but the measurements are not very reliable. Cousteix *et al.* (1981) did observe that the turbulence structure was affected by oscillation. However, they did not make wall-shear-stress measurements, which are essential for the understanding of the flow at high frequencies. The experiments of Mizushina *et al.* (1975), Ramaprian & Tu (1980) and the present experiments are the only ones in this regime that provide details of the flow structure. The data of Mizushina *et al.* largely agree with the present measurements, but do not contain wall-shear-stress measurements. In fact, more measurements of wall shear stress are needed to strengthen the observations made in the present study.

5. Conclusions

The following are the major conclusions that can be drawn from the study reported in this paper.

(1) The Stokes number Ω used to characterize periodic laminar pipe flow is not appropriate for describing the periodic turbulent pipe flow. In fact, the effect of

unsteadiness in periodic turbulent flow spreads over a distance that can be several orders of magnitude larger than the thickness $(2\nu/\omega)^{1/2}$ of the conventional Stokes layer for the same frequency. The analogous parameter characterizing (at least the outer part of) the unsteady turbulent flow is $\omega D/U_*$, which can be called the 'turbulent Stokes number'. This number has the primary significance of being proportional to the ratio of the pipe radius to the turbulent diffusion distance in one oscillation period. However, it turns out that this parameter can also be used to study, at any given Reynolds number, the interaction of the imposed oscillation with the turbulent bursting process. Using this parameter, the imposed oscillation in periodic turbulent shear flows can, in principle, be classified into five regimes, namely quasi-steady, low-frequency, intermediate-frequency, high-frequency and rapid-oscillation.

(2) The maximum phase shift of wall shear stress (relative to the cross-sectional-average velocity) over the frequency range studied (intermediate and high) is of the order of 10° , which is considerably less than that in laminar flow. The phase angle of the velocity is completely different in distribution from that in laminar flow at the same oscillation frequency. Ensemble-averaged turbulence intensities and Reynolds shear stress experience very large phase shifts. These phase shifts increase with the oscillation frequency. The turbulence properties are thus delinked from the local flow both in the intermediate- and high-frequency ranges.

(3) Spectral measurements show that turbulent frequencies smaller than the imposed oscillation frequency will be attenuated. Consequently, the integral timescale will be smaller in the unsteady flow than in steady flow at the same time-mean Reynolds number.

(4) The ensemble-averaged rate of turbulent-energy production appears to undergo drastic changes during the cycle at the intermediate frequency of oscillation. It is more or less frozen and resembles steady-flow behaviour at the high frequency of oscillation.

The present study was supported by the U.S. Army Research Office Grant DAAG29-79-G-0017, and the authors gratefully acknowledge this support.

REFERENCES

- ACHARYA, M. & REYNOLDS, W. C. 1975 Measurements and predictions of a fully developed turbulent channel flow with imposed controlled oscillations. *Stanford Univ. Thermosci. Div. Tech. Rep.* TF-8.
- BENDAT, J. S. & PIERSOL, A. G. 1971 *Random Data: Analysis and Measurement Procedures*. Wiley-Interscience.
- BINDER, G. & KUENY, J. L. 1981 Measurements of the periodic velocity oscillations near the wall in unsteady turbulent channel flow. In *Unsteady Turbulent Shear Flows* (ed. R. Michel, J. Cousteix, & R. Houdeville), pp. 100–108. Springer.
- COUSTEIX, J., HOUEVILLE, R. & JAVELLE, J. 1981 Response of a turbulent boundary layer to a pulsation of the external flow with and without adverse pressure gradient. In *Unsteady Turbulent Shear Flows* (ed. R. Michel, J. Cousteix & R. Houdeville), pp. 120–144. Springer.
- HINO, M., SAWAMOTO, J. & TAKASU, S. 1976 Experiments on transition to turbulence in oscillatory pipe flow. *J. Fluid Mech.* **75**, 193–207.
- HINZE, J. O. 1959 *Turbulence*. McGraw Hill.
- KARLSSON, S. F. 1959 An unsteady turbulent boundary layer. *J. Fluid Mech.* **5**, 622–636.
- KIRMSE, R. E. 1979 Investigations of pulsating turbulent pipe flow. *Trans. ASME*, 79-WA/FE-1.
- KITA, Y., ADACHI, Y. & HIROSE, K. 1980 Periodically oscillating turbulent flow in a pipe. *Bull. JSME* **23**, 656–664.

- KOBASHI, Y. & HAYAKAWA, M. 1981 Structure of turbulent boundary layer on an oscillating flat plate. In *Unsteady Turbulent Shear Flows* (ed. R. Michel, J. Cousteix and R. Houdeville), pp. 67–76. Springer.
- LAWN, C. J. 1971 The determination of the rate of dissipation in turbulent pipe flow. *J. Fluid Mech.* **48**, 477–505.
- MIZUSHINA, T., MARUYAMA, T. & HIRASAWA, H. 1975 Structure of the turbulence in pulsating pipe flows. *J. Chem. Engng Japan* **8**, 210–216.
- MIZUSHINA, T., MARUYAMA, T. & SHIOZAKI, Y. 1973 Pulsating turbulent flow in a tube. *J. Chem. Engng Japan* **6**, 487–494.
- OHMI, M., USUI, T., TANAKA, O. & TOYAMA, M. 1976 Pressure and velocity distribution in pulsating turbulent pipe flow. *Bull. JSME* **19**, 951–957.
- RAMAPRIAN, B. R. & TU, S. W. 1980 An experimental study of oscillatory pipe flow at transitional Reynolds numbers. *J. Fluid Mech.* **100**, 513–544.
- RAMAPRIAN, B. R. & TU, S. W. 1982 Study of periodic turbulent pipe flow. *IIHR Rep.* 238, Iowa Inst. of Hydraul. Res.
- SIMPSON, R. L., SHIVAPRASAD, B. G. & CHEW, Y. T. 1981 Some features of unsteady separating turbulent boundary layers. In *Unsteady Turbulent Shear Flows* (ed. R. Michel, J. Cousteix & R. Houdeville), pp. 109–119. Springer.
- TU, S. W. & RAMAPRIAN, B. R. 1983 Fully developed periodic turbulent pipe flow. Part 1. Main experimental results and comparison with predictions. *J. Fluid Mech.* **137**, 31–58.
- UCHIDA, S. 1956 The pulsating viscous flow superposed on the steady motion of incompressible fluid in a circular pipe. *Z. angew. Math. Phys.* **7**, 403–421.